Received: 9 November 2023 | Revised: 5 February 2024 | Accepted: 9 February 2024

DOI: 10.1002/bip.23571

ARTICLE

Biopolymers WILEY

Correlation between the activation energy of PLA respectively PLA/starch composites and mechanical properties with regard to differ accelerated aging conditions

Margarita Reit | Jan-Christoph Zarges | Hans-Peter Heim

Institute of Material Engineering, Polymer Engineering, University of Kassel, Kassel, Germany

Correspondence
Margarita Reit, Institute of Material Engineering, Polymer Engineering, University of Kassel, Mönchebergstraße 3, 34125 Kassel, Germany.
Email: reit@uni-kassel.de

Funding information
Bundesministerium für Ernährung und Landwirtschaft; Fachagentur Nachwachsende Rohstoffe e.V. (FNR), Grant/Award Number: 2220NR089E

Abstract

Within this research semi-crystalline polylactide and composites with 50 wt.% native potato starch were compounded and injection molded. The material was mechanically characterized by tensile, three-point bending, and Charpy impact tests. These tests were carried out in the freshly molded state and after 332 and 792 h of storage at accelerated temperature or humidity. The respective activation energy was calculated by applying the Flynn-Wall-Ozawa method. The focus of the study was to investigate the correlation between the activation energy and the related mechanical and thermal properties. The results showed that the addition of native potato starch as a filler prevents the decrease in activation energy over the course of the experiments. Thus, the PLA/starch composite is more resistant to the two aging conditions than the pure PLA. When considering the mechanical properties, the pure PLA showed a large deviation of results compared to the initial value in a range of +63.88% to −33.96% with regard to the respective aging conditions, whereas the PLA/starch composite properties nearly always remained at the initial values. Through the investigation of the mechanical and thermal properties, it was shown that the steady activation energies are consistent with the mechanical properties, as these have shown only a small deviation of the mechanical properties during the duration of experiments for the PLA/starch composite.

KEYWORDS
activation energy, Flynn-Wall-Ozawa, native potato starch, polylactide, resistance, thermal degradation, thermogravimetric analysis (TGA)

1 | INTRODUCTION

Bioplastics are increasingly gaining importance due to the increased exchange from commonly used petroleum-based plastics to bioplastics. Among the bioplastics, the most promising and widely spread bioplastic is polylactide (PLA).[1,2] PLA has become part of our everyday life and has already been investigating in numerous publications with different research aspects like medical applications or the packaging industry.[3–8] However, one challenge so far is the investigation of the long-term durability especially because PLA is often used for packaging or single-use products.[9,10] To enlarge the field of application for PLA appropriate research regarding durability is necessary. The durability or service lifetime is one of the main characteristics of a material where service lifetime is the time during which the material can be

used to maintain its properties in accordance with its field of application.[11] Unfortunately, lifetime investigations are very time-consuming due to the long duration of experiments. In order to obtain data on the long-term behavior of materials accelerated aging is performed. Accelerated aging is performed at selected accelerated aging conditions. The assumption underlying accelerated aging is usually the Arrhenius equation which implies that an increase in temperature leads to accelerated chemical reactions.[11] The Arrhenius equation includes the variable activation energy E_a. This energy is considered an energy barrier that has to be overcome for a chemical reaction to take place.[12] The lower the E_a, the faster the chemical reaction occurs. Due to the fact that chemical degradation is irreversible, the E_a regarding Arrhenius equation is a suitable parameter for determining the effects of aging.[13–15] In order to correlate the effects of aging and the calculated E_a with the mechanical properties, the elongation at break and impact strength are taken into account. Both parameters have already been used in a number of publications to characterize the influence of aging on the material.[16–20]

Since a responsible and sustainable use of available resources is important, PLA is often used as a composite by adding filler materials. PLA composites have already been investigated in the scope of cork/poly-lactic acid[21] or pineapple leaf fiber/poly-lactic acid.[22] Another more commonly used filler material is starch. Starch is characterized by the fact that it is available in large quantities making it renewable since starch is extracted from plants and has a quite easy biosynthetic pathway.[23] The study of Acioli-Moura et al.[24] proved the significant reduction of mechanical properties of PLA and PLA/starch composites after storage in accelerated relative humidity. As well as the aim of this study is to prove an increase E_a by adding starch as a filler, publications by Moraczewski et al.[25] have already shown that the addition of various extracts increases the resistance of PLA. Other studies have already shown that the addition of bamboo particles into PLA led to an increase in the E_a.[26] Abderrahim et al.[27] have already shown that adding fillers such as cellulose fibers to PBS increases the activation energy and thus make the material more resistant.

In other publications, the dependence of various properties such as the glass transition temperature,[28] particle size,[29] or conductivity[30] and the E_a were investigated. The present work studies the effect of improved resistance to various aging influences by adding starch as a filler material in PLA composites with respect to the activation energy and the related mechanical properties. Bio-based PLA composites with a native potato starch content of 0 and 50 wt.% were fabricated. The injection molded test specimens were aged at accelerated temperature and humidity. For reference, test specimens were stored in a standardized climate. Subsequently, the test specimens were characterized thermally and mechanically. The related activation energy was calculated using the Flynn-Wall-Ozawa method. The same composite has already been studied in Reference [31] but under different environmental conditions.

2 | MATERIALS AND METHODS

2.1 | Matrix and filler

For the investigations, semi-crystalline PLA Luminy® L130 provided by TotalEnergies Corbion (NS Gorinchem, Netherlands) with a density of 1.24 g/cm^3 and a melting temperature of 175°C was used. To analyze the correlation between E_a and the mechanical properties native potato starch type Superior from the company Emsland Stärke (Emlichheim, Germany) was used for the composites. Images under the light-transmitted microscope of the starch have shown mostly round or oval shapes of the native potato starch grains. The measured size was about 20 µm up to 70 µm. In the following native potato starch is called starch.

2.2 | Preparation of the composite

The PLA/starch composite with 50 wt.% starch was produced using a twin-screw-extruder ZSE 18 HPE by Leistritz Extrusionstechnik GmbH (Nuremberg, Germany) with a screw-diameter of 18 mm and a process length of 40 D. The PLA was dried before compounding using a compressed air dry air dryer (TORO-systems; Ingensdorf, Germany) for 6 h at 100°C while starch was dried in a convention oven for 6 h at 105°C.[32] No additives or coupling agents were used. The temperature settings are shown in Table 1. After cooling down the strand was granulated (3–4 mm) with an Altivar ATV31C075M2 (Ratingen, Germany).

2.3 | Injection molding

The test specimens according to DIN EN ISO 527-2-1A were produced using the injection molding machine Allrounder 320C from Arburg GmbH & Co. KG (Lossburg, Germany) with a screw diameter of 25 mm and a clamping force of 500 kN. Prior to the injection molding the material was dried for 6 h at 100°C. The dimensions of the test specimen are shown in Figure 1.

Processing temperatures are shown in Table 2. Further parameters were a cycle time of approx. 98 s with a holding pressure drop from 700 to 500 bar within a time of 25 s. The mold temperature was set to 30°C.

TABLE 1 Temperature profile used in the compounding process.

Zone	1	2	3	4	5	6	7	Nozzle
Temperature in °C	165	165	175	185	185	185	195	195

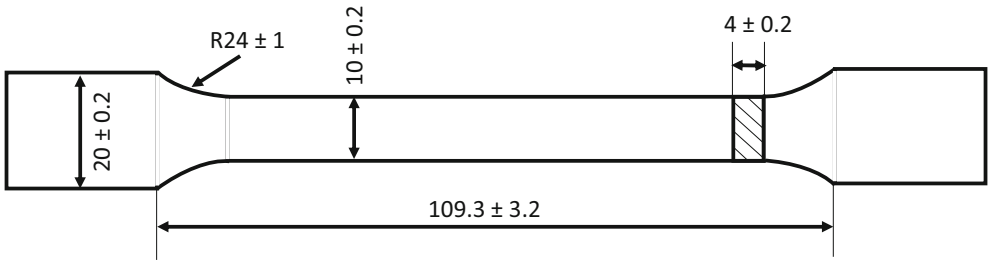

FIGURE 1 Dimensions of evaluated test specimen according to DIN EN ISO 527-2.

TABLE 2 Temperature profile used in the injection molding process.

Zone	1	2	3	4	5	Nozzle
Temperature in °C	200	205	210	215	215	215

TABLE 3 All three aging conditions under which the test specimens were aged.

Accelerated aging	Temperature in °C	Relative humidity in %
Standardized climate	23	50
High humidity	23	75
High temperature	70	10

2.4 | Accelerated aging

Three different aging conditions were selected to investigate the change in the E_a under different environmental conditions. Therefore, an accelerated aging regarding elevated temperature and relative humidity was selected. For this purpose, the climate chambers ATLAS SolarClimate SC340 MHG by Weiss Technik GmbH (Reiskirchen, Germany) and KPK 400 by Feutron Klimasimulation GmbH (Langenwetzendorf, Germany) were used. For reference purposes, test specimens were aged under a standardized climate according to DIN ES ISO 291. To investigate the change of the E_a and the material properties depending on the time, the test specimens were investigated at a freshly molded condition and after 168 and 504 h of accelerated aging. After the accelerated aging the test specimens were stored another 168 h in standard climate. In Table 3, the conditions during the storages are listed.

For the purpose of consistency, the abbreviations FM for freshly molded, SC for standard climate, TE for accelerated temperature storage and HU for accelerated humidity are defined in the following. The storage times can be found in Table 4.

2.5 | Tensile test

Tensile tests were carried out to investigate the correlation between E_a and elongation at break. For this purpose, test specimens were characterized using the universal testing machine Z010 by Zwick Roell (Ulm, Germany) according to DIN EN ISO 527 at a speed of 5 mm/min. The parameters of Young's modulus, tensile strength, and elongation at break were determined. A total of five test specimens per batch were analyzed.

TABLE 4 All three aging conditions and the corresponding storage time.

Aging conditions	Storage time 1	Storage time 2	Total storage time
Standardized climate	792 h	1002 h	1002 h
High humidity	168 h plus 168 h SC	504 h plus 168 h SC	332 h
High temperature	168 h plus 168 h SC	504 h plus 168 h SC	792 h

2.6 | Three-point bending test

For the three-point bending test 80 × 10 × 4 mm^3 specimens were cut out of type 1A tensile specimens. The tests were carried out according to DIN EN ISO 178 on a Zwick Roell Z010 Universal Testing Machine (Ulm, Germany) with a distance between the supports of 64 mm. A total of five test specimens per batch were analyzed.

2.7 | Charpy impact test

According to DIN EN ISO 179 Charpy impact tests were conducted. Test specimens of the following dimensions 80 × 10 × 4 mm^3 were cut out of type 1A specimens. For the test, a Zwick Charpy impact machine with a 5 J hammer was used. A total of five test specimens per batch were analyzed.

2.8 | Thermogravimetric analysis (TGA)

TGA measurements were processed on a TGA-Modul Q 500 (TA Instruments) with sample weights of approx. 20 mg. Samples were heated at heating rates of 10, 20, and 30 K/min from room temperature (means 23°C) to 600°C under a nitrogen gas flow rate of 40 cm^3/min. TA Universal Analysis Program was used for evaluating the data.

2.9 | Flynn-Wall-Ozawa (FWO)

To obtain the activation energy E_a using TGA measurements the integral method proposed by Flynn-Wall-Ozawa (FWO)[33–35] was chosen. The calculation of the energy is based on the mass loss during heating in the TGA at different heating rates. The advantage of this method is that no prior knowledge of the reaction mechanism is required. The formula of the thermal degradation process states:

$$\log\beta = \log\frac{AE_a}{g(\alpha)R} - 2.315 - \frac{0.4567E_a}{RT}, \quad (1)$$

where β is the heating rate, A is a pre-exponential factor, $g(\alpha)$ is the integral mechanism function $g(\alpha) = \int_0^\alpha d\alpha/f(\alpha)$ and R is the gas constant $\left(8.314\,\mathrm{J\,mol^{-1}K^{-1}}\right)$.[36] The E_a is calculated by plotting the $\log(\beta)$ against $1/T$. The resulting straight line with the corresponding slope is proportional to the E_a. The slope is determined for different degrees of the conversion then an average E_a is calculated. The conversion degree is determined using:

$$\alpha = \frac{W_0 - W_t}{W_0 - W_f} \quad (2)$$

Here W_0 is the initial weight, W_t is the weight at time t and W_f is the final weight.[36]

2.10 | Differential scanning calorimetry (DSC)

As the property changes of a material are depending on the crystallinity dynamic differential scanning calorimetry measurements (DSC) according to DIN EN ISO 11357 were carried out. Therefore, the DSC module Q2000 (TA Instruments, New Castle, USA) was used with a constant heating rate of 10 K/min (sample weight approx. 10 mg) and under a nitrogen atmosphere with a temperature program of 0–250°C. As the focus of this research is the aging of the material only the first heating cycle was investigated. The crystallization $X_c[\%]$ was calculated regarding Equation (3) using the enthalpy of fusion (ΔH_f), the enthalpy of crystallization (ΔH_c) and the mass fraction of the matrix (w). For 100% crystallinity a value of 93.6 J/g (ΔH^0_f) for PLA was chosen.[37–39]

$$X_c[\%] = \frac{\Delta H_f - \Delta H_c}{w \cdot \Delta H_f^0} \cdot 100, \quad (3)$$

In addition to crystallinity, the glass transition temperature T_g was also evaluated using the program TA Universal Analysis.

2.11 | Microscopy

In order to investigate the crystalline structure of the material transmission light microscopy was used. Thin section images were taken with the microscope Keyence VHX-600, VH-Z20. For the detailed analysis of the crack structure, the 3D laser scanning-microscope VK-X3000 (Keyence, Osaka, Japan) was used.

3 | RESULTS

3.1 | Activation energy of PLA and PLA/starch

Figure 2 shows the linear fitting plots of $\log(\beta)$ against $1/T$ for the FWO method for PLA/starch in a standardized climate after 792 h. The lines, which belong to the conversion rates of 95 to 15 are parallel and are close to each other, confirming the application of the FWO method. The line for a high conversion rate of 99 indicates a different slope and is showing no parallel behavior to the other lines. Also, the low conversion rate line of 5 shows a different pattern. If the remaining measurements are considered, the fitting lines at 25 and 15 in particular show a similar behavior. In order to consistently use the same conversional values for the calculation an α from 0.35 to 0.95 was chosen. This non-parallelism of the lines greatly influences the calculated E_a. Those fitting lines at the beginning or end of the measurement can be explained by the moisture of the material in the beginning or the rest burned starch in the crucible. As the measurement was done twice the deviation was only about ±4°C.

The change in the calculated E_a depending on the storage is shown in Figure 3. In Figure 3a, the E_a for the three different storage conditions of pure PLA and (b) the E_a of PLA/starch are shown. For the initial value, the E_a of the freshly molded state was taken. The E_a was then calculated for the accelerated aged test specimens. For conditioning, the samples were placed in the standard climate for 168 h right after accelerated aging.

For the pure PLA test specimens, a rapid decrease in the E_a after temperature of 24.07% and humidity storage of 29.63% can be seen after the first 168 h. Thereafter, the E_a continues to decrease, with a more pronounced drop after temperature storage of 40.12%. In the

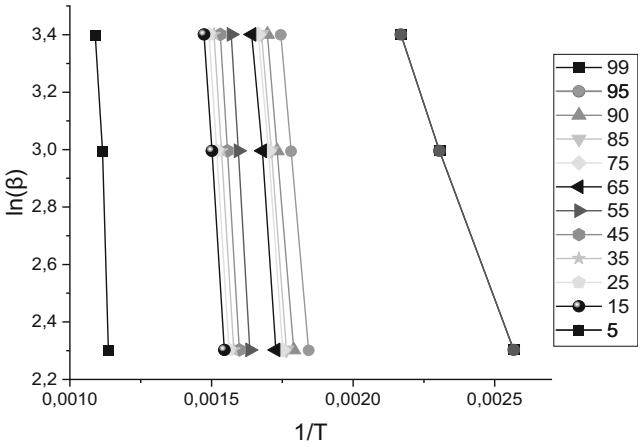

FIGURE 2 Flynn-Wall-Ozawa linear plots at three different heating rates for different conversion of PLA_50_SC.

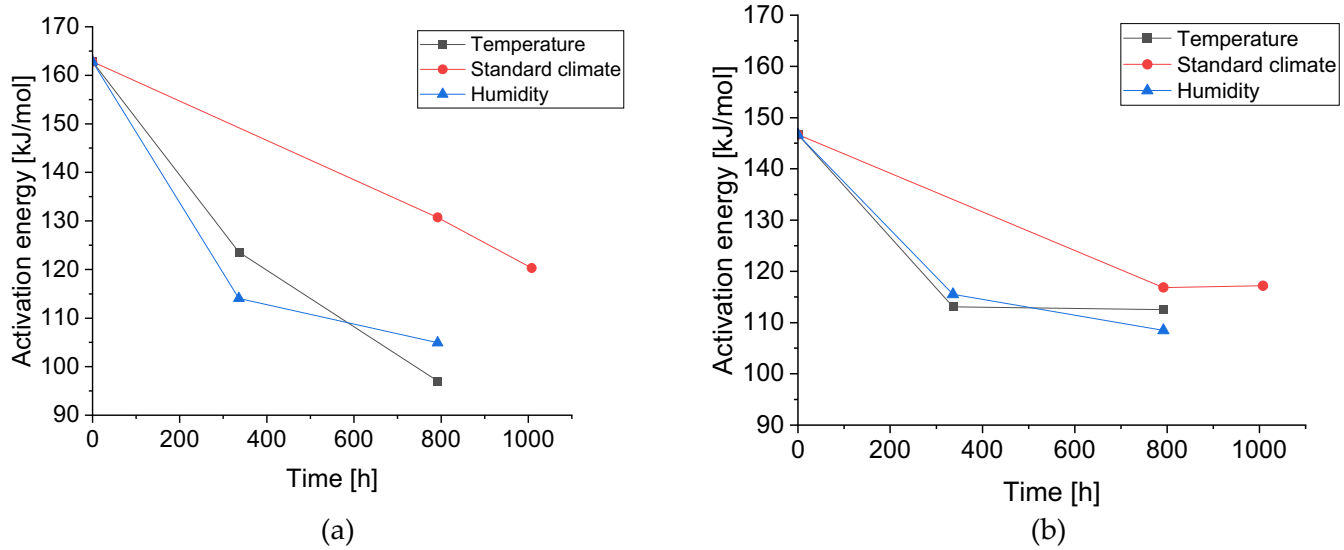

FIGURE 3 Change of E_a regarding the three aging conditions: (a) PLA; (b) PLA/starch composite.

standard climate, the E_a also decreases by 25.93%. This indicates that the accelerated aging conditions affect the PLA more than in the standard climate. As with pure PLA, a decrease in the E_a can be seen for PLA/starch in Figure 3b due to the two accelerated aging conditions within 332 h. Thereafter, the E_a is approximately constant after 792 h of temperature storage (from 22.6% to 23.29%) and only slightly decreased during humidity storage (from 20.55% to 19.86%). In standard climate the E_a remains nearly constant from 792 to 1002 h (from 21.23% to 26.03%). Unlike pure PLA where the different aging conditions led to a clear decrease of the E_a during the storage time, the PLA/starch composite maintained a similar value for the E_a after 332 h, respectively, 792 h. The storage conditions, therefore, do not affect the composite material as much as the pure PLA.

In Table 5, all values of E_a from Figure 3 are listed with the mean value of the coefficient of determination. This is the characteristic value of whether the straight line approximates the measured values from the three heating rates.

To analyze the degradation behavior of pure PLA and PLA/starch composites in Figure 4 the TGA curves are illustrated. The TGA curves of the pure PLA are shown in black with typically sigmoid curves. Thermal degradation occurs more rapidly, or the temperature at which PLA begins to degrade is lower in the aged test specimens when compared to specimens subjected to standard climate. Also, as with the analysis the E_a, it can be seen that accelerated aging affects the material more than aging in a standard climate. If the TGA curves of the PLA/starch are considered (Figure 4, blue), the sooner beginning or the lower temperature, from which thermal degradation starts, is noticeable. Similarly, as for the pure PLA, it is evident that the specimen from accelerated aging starts to degrade earlier.

In light blue in Figure 4, the TGA curve of pure starch is plotted. Up to 150°C a strong mass loss occurs due to evaporating humidity. From 270 to 300°C, the second strong mass loss takes place. Above this temperature, the pure starch degrades.

TABLE 5 Calculated E_a of PLA and PLA/starch composite regarding all three aging conditions and storage times.

Specimen name	Wt.%.	Storage time in h	E_a in J/mol	R^2
PLA_0_FM	0	0	162.78	0.9856
PLA_50_FM	50	0	146.68	0.9652
PLA_0_TE_332	0	332	123.56	0.9983
PLA_0_TE_792	0	792	97.03	0.9948
PLA_50_TE_332	50	332	113.08	0.9958
PLA_50_TE_792	50	792	112.53	0.9982
PLA_0_HU_332	0	332	114.07	0.9978
PLA_0_HU_792	0	792	104.92	0.9981
PLA_50_HU_332	50	332	115.52	0.9976
PLA_50_HU_792	50	792	108.47	0.9975
PLA_0_SC_792	0	792	130.72	0.9731
PLA_0_SC_1008	0	1008	120.31	0.9854
PLA_50_SC_792	50	792	116.85	0.9756
PLA_50_SC_1008	50	1008	117.19	0.9867

When analyzing the TGA curve of the PLA/starch composite with respect to the temporal evolution of mass loss, three distinct phases or peaks of mass loss become evident. The initial phase occurs within the temperature range of 270–330°C. As it was established beforehand that starch degrades prior to pure PLA, this likely corresponds to the degradation of starch within the PLA/starch composite. The subsequent significant degradation takes place between 330 and 380°C, primarily involving the pure PLA component. Finally, at 600°C, there is a subsequent increase in the derivative of mass loss, attributed to the residual starch remaining in crucible. In the temperature range between 400 and 600°C, the composite curve can be seen to lie exactly between the black pure PLA and light blue pure starch curve.

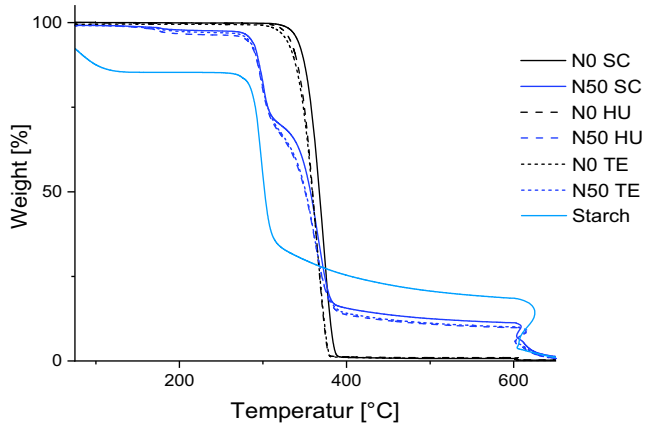

FIGURE 4 TGA curves of PLA and PLA-Starch after 504 h of SC, TE and 729 h HU aging (heating rate = 10 K/min).

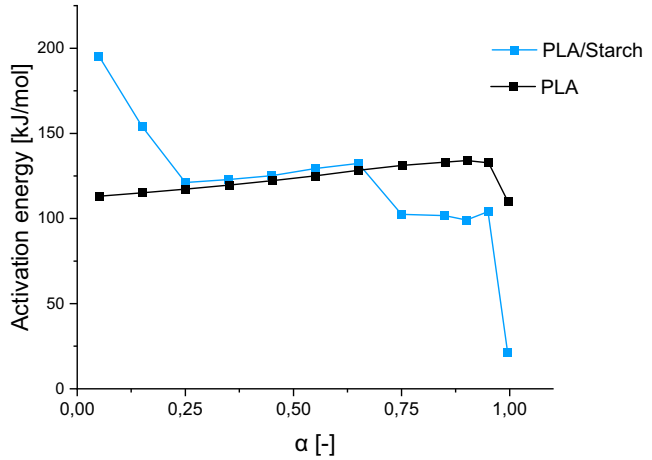

FIGURE 5 Change of the E_a of PLA and PLA/starch in standard climate (792 h) for different conversion rates.

This corresponds to the 50% starch content in the composite. If these three different material mass losses are compared with each other, it is clear that the faster degradation of the composite is caused by the starch in the PLA/starch composite.

If considering the single components of the PLA/starch composite and the correlation between the degradation of these components, Figure 5 presents the energy vs. conversion rate.[40] The E_a of pure PLA barely changes depending on the conversion rate. The PLA/starch composite reflects the results from Figure 4 and three different phases. At low α, the E_a is large, then settles to the value of the E_a of the pure PLA at middle α and shows a small E_a at high α. The diagram thus reflects that the degraded starch in the composite at the beginning of the degradation leads to high E_a. The small amount of residual soot then leads to a strong decrease in E_a at low α.

3.2 | Mechanical properties

The elongations at break from the tensile tests can be seen in Figure 6. The freshly molded pure PLA samples have an average

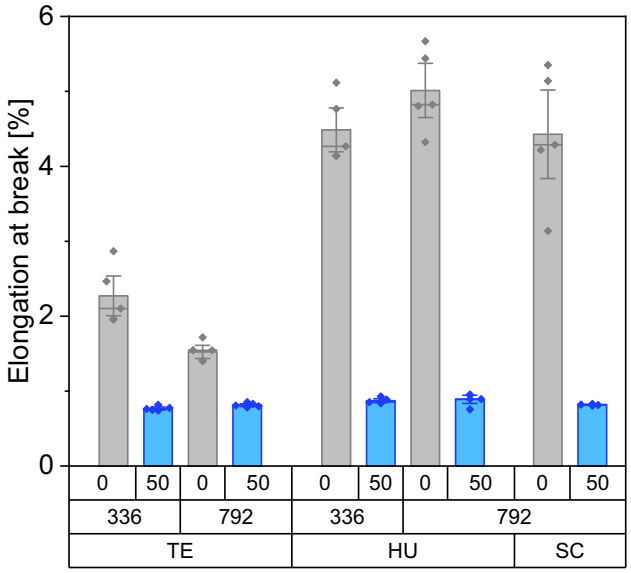

FIGURE 6 Elongation at break during tensile test of PLA (gray) and PLA/starch (blue) of all three aging conditions and times.

elongation at break of 84.4% and are not shown in the diagram. All storage conditions cause a strong decrease of elongation at break compared to the freshly molded condition. The accelerated temperature leads to a decrease by 33.04% of the elongation at break from 2.27% to 1.52% after 792 h. The opposite behavior is shown by the results of the humidity storage. The elongation at break increases by 11.58% in the course of the storage time from 4.49% to 5.01%. In the standard climate, the elongation at break is in the range of the humidity-stored specimens after 168 h. For the starch-containing specimens, no great difference in elongation at break over the storage period is evident under any of the storage conditions. The greatest deviation from the initial value of 0.91% elongation at break in the freshly molded state is observed after 336 h of temperature storage to 0.77%, meaning a decrease of 15.38%. The least deviation (2.2%) is after 792 h in humidity storage from 0.91% to 0.89%.

Figure 7 shows the elongation at break from the three-point bending test. Over the duration of temperature storage, the elongation at break decreases by 34.54% after 792 h compared to the 336 h stored samples, from 3.85% to 2.53%. In the humidity aging, the elongation increases by 38.41% over the 792 h from 8.19% to 11.35%. An increase in the value can also be seen in the standard climate (55.23%) from the freshly molded value of 6.82% to 10.59%. As with the elongation at break from the tensile test, the results of the starch-containing specimens overall conditions show no great difference during storage time. During temperature storage, the value increased by 4.03% from 1.24% at 336 h to 1.29% at 792 h. In humidity storage, the value increases by 12.16% from 1.48% to 1.66%. In comparison, the elongation at break of the standard climate stored samples increased by 2.9% from 1.38% to 1.42% compared to the freshly molded condition.

The last mechanical property to be mentioned is the impact strength, as seen in Figure 8. Compared to the fresh injection molded state, the impact strength of the pure PLA samples increased strongly by 222.70% during the temperature storage. The impact strength

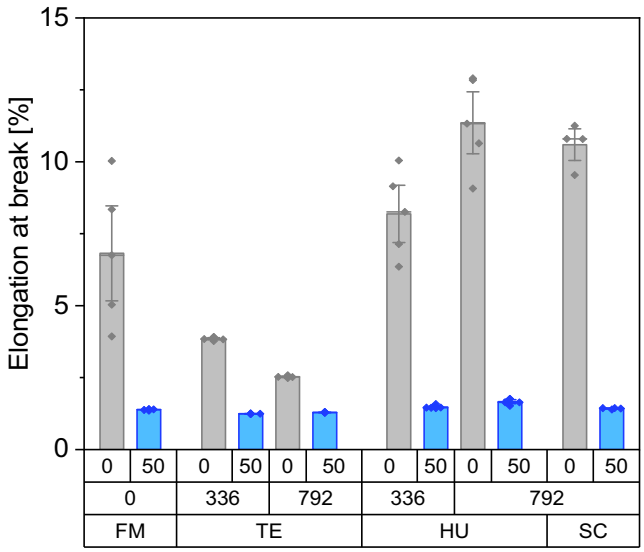

FIGURE 7 Elongation at break during three-point bending modulus of PLA (gray) and PLA/starch (blue) of freshly molded state and all three aging conditions.

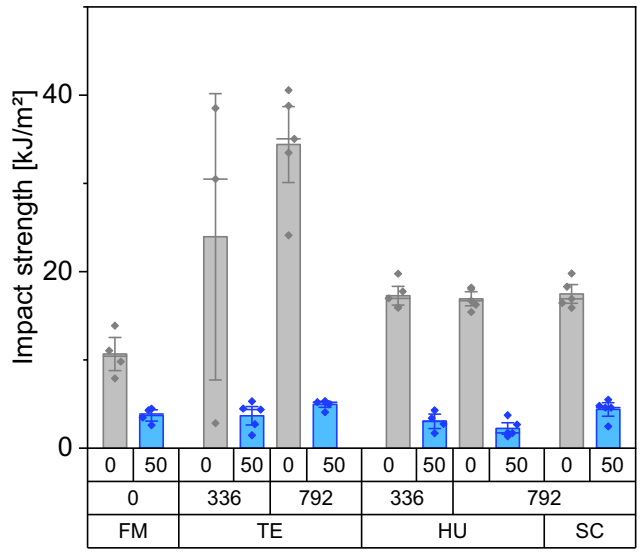

FIGURE 8 Impact strength of PLA and PLA/starch regarding freshly molded state and all three aging conditions.

increases by 58.82% during storage in a humidified condition. After 792 h in the standard climate, there is also an increase (63.88%) in impact strength. For the starch-containing specimens, a slight increase of 33.96% in impact strength is seen after 792 h with respect to temperature storage. In the humidity storage, in turn, a slight drop of 39.62% in impact strength can be seen. The standard climate leads to a slight increase (18.33%) in impact strength.

3.3 | Differential scanning calorimetry (DSC)

DSC measurements were employed to assess crystallinity, a factor known to exert a significant impact on material properties. The computed values are presented in Table 6. In addition to crystallinity, Table 6 also provides the glass transition temperature T_g. Notably, in the case of pure PLA, the degree of crystallization diminishes during exposure to standard climate conditions and humidity storage, while it experiences a subsequent increase during temperature storage. The increase in crystallinity due to the increased temperature is caused by the increased mobility of the molecules. The molecular chains can arrange in a crystallographic structure.[41] The decrease in the crystallinity of the two other storage conditions is influenced by the humidity. The humidity tends to promote a dissolving of the crystalline structure as water molecules diffused into the material and weaken the hydrogen bonds.[42] The lower degree off crystallization of the standard climate compared to the freshly molded value is within the standard deviation of the measuring device. For PLA/starch composites, the crystallinity increases in the humidity storage and especially strongly in the temperature storage, but decreases in standard climate. The increase in all storages is due to the nucleating effect of the starch.[31,43] This effect is even more noticeable in temperature storage, as the proportion of pure PLA also increases due to the higher temperature. Considering the T_g, there is a decrease in the T_g of the pure PLA in humidity storage. In temperature storage, T_g increases after 332 h but decreases again after 792 h. The PLA/starch exhibits a lower T_g than the pure PLA in the freshly molded state and also after 792 h in the standard climate. In humidity storage, the T_g increases slightly and remains almost the same in temperature storage.

TABLE 6 Calculated crystallinity degree and glass transition temperature of aged and unaged samples.

Specimen name	*K*% in %.	T_g in °C
PLA_0_FM	14.6	64.94
PLA_0_HU_332	5.7	58.69
PLA_0_HU_792	11.7	61.38
PLA_0_TE_332	41.4	79.88
PLA_0_TE_792	43.1	57.67
PLA_0_SC_792	11.9	60.66
PLA_50_FM	15.4	58.75
PLA_50_HU_332	22.8	61.85
PLA_50_HU_792	24.6	59.83
PLA_50_TE_332	30.1	61.23
PLA_50_TE_792	35.4	58.62
PLA_50_SC_792	7.9	58.48

3.4 | Transmission light microscopy

As the results of the DSC indicated a high increase of the crystallinity after the storage at accelerated temperature this relationship was investigated with thin section images in the transmitted light. As shown in Figure 9a, the thin section image of pure PLA after 504 h at accelerated humidity showed no structures at all. The accelerated temperature in contrast is revealing a crystalline structure except the

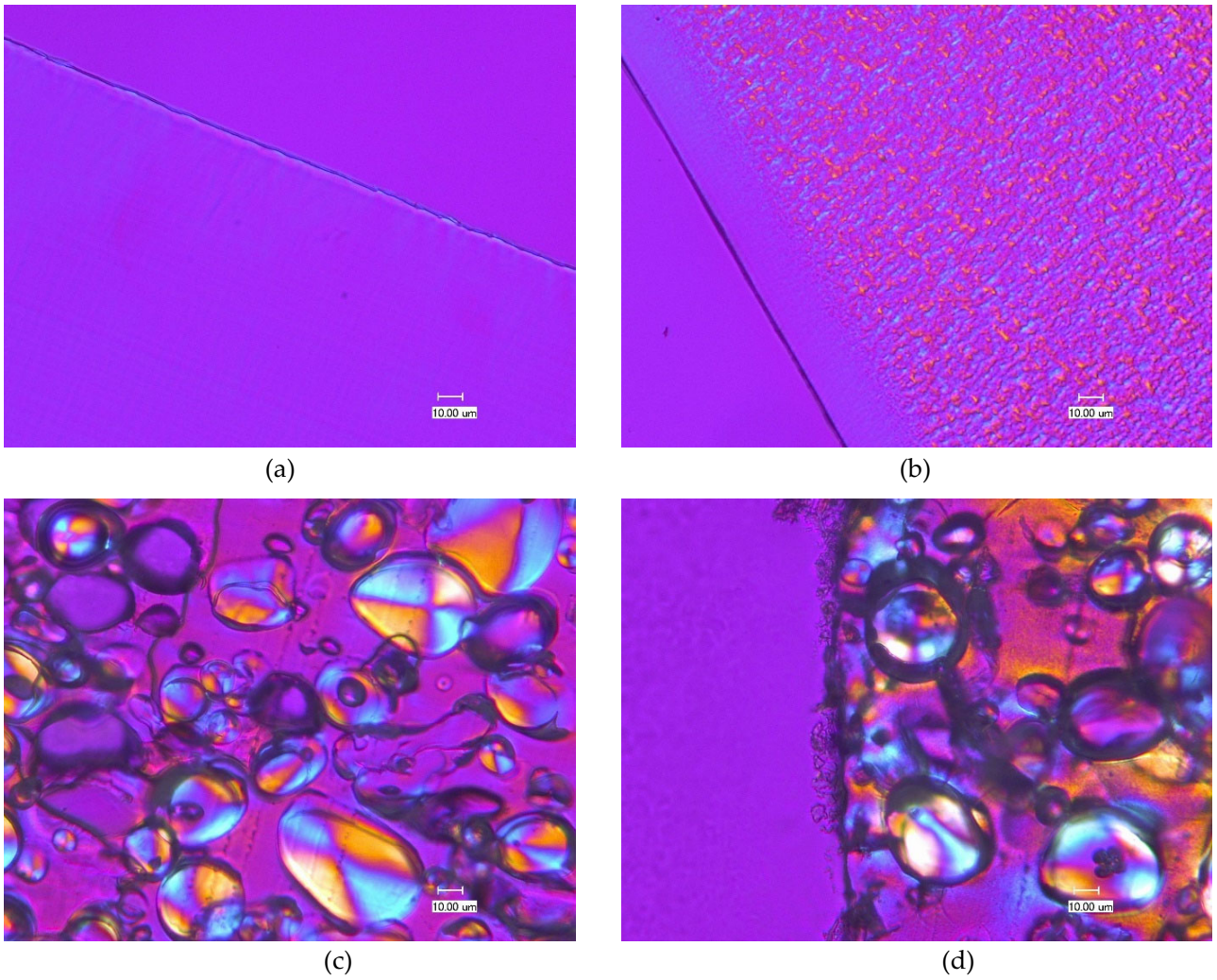

FIGURE 9 Thin section images in transmitted light of: (a) PLA 0 w% at humidity storage; (b) PLA 0 w% at temperature storage; (c) PLA 50 wt.% at humidity storage and (d) PLA 50 wt.% at temperature storage.

FIGURE 10 Test specimens after all four storage conditions: (a) pure PLA, (b) composite. 1 is freshly molded, 2 after standard climate, 3 after temperature storage and 4 after humidity storage.

edge area (Figure 9b). The thin section images of the PLA/starch composite showed a similar result. The storage at accelerated temperature showed no crystalline structure, only the starch grains showed the typical Maltese cross. In the accelerated temperature sample, color changes can be seen in the matrix material surrounding the starch grains. These also indicate a crystalline structure similar to figure b.

Figure 10a shows the pure PLA test specimens. Specimen 1 is freshly molded, sample 2 was stored in standard climate, 3 in

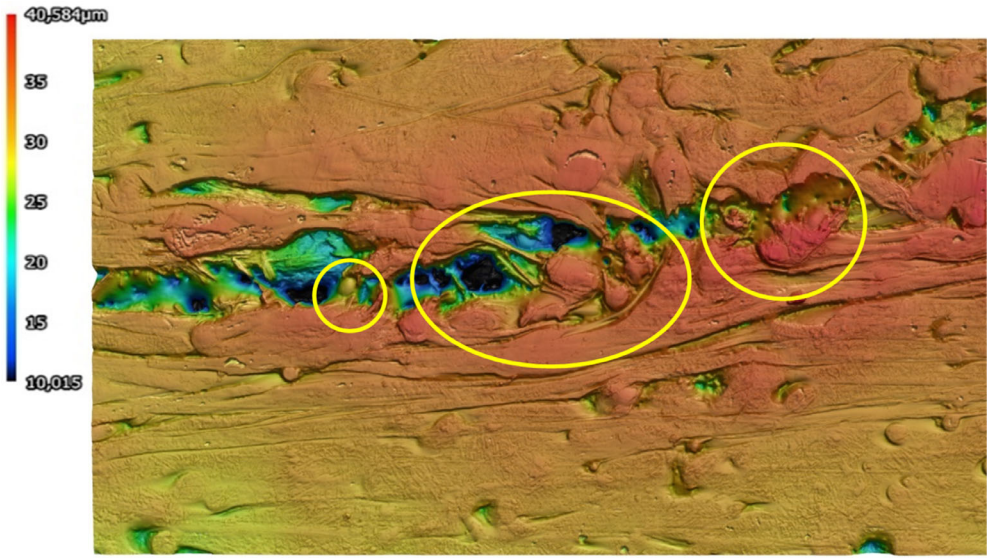

FIGURE 11 3D laser scanning microscope of a crack in a humidity stored PLA/starch composite test specimen.

temperature and 4 humidity stored. Sample 3 in particular stands out. The material shows a strong change in color and is no longer transparent. The change in structure reflects the DSC results and the increased degree of crystallization. Figure 10b shows the composite test specimens. The storage conditions correspond to those in Figure 10a. A turbidity of sample 3 can be seen. This shows the increase in the crystalline percentage of the material, see results Table 6. The difference between the temperature-stored samples and the humidity-stored samples, is that sample 4 shows cracks. The swelling and release of the humidity led to the formation of crack structures.

In order to show more precisely the areas in which the cracks occur in the starch-containing test specimens, a crack is shown in Figure 11 using the 3D laser scanning microscope. Starch grains can be seen in the marked areas. The clear separation of the PLA and the starch granules is clearly visible. It can also be seen that the cracks predominantly occur along the grain accumulations.

4 | DISCUSSION

In the course of the studies, improved resistance against various aging conditions of PLA in combination with starch was demonstrated. This effect could be determined based on the calculated activation energy using thermogravimetric measurements. The addition of starch as a filler in PLA led to the result that under all three aging conditions, that is, accelerated temperature or humidity and standard climate, the E_a did not decrease as rapidly or at all in the course of the storages in comparison with pure PLA. The starch as filler in PLA slowed down the change in E_a during the experiments. The evaluation of the TGA curves showed that the PLA/starch composite has a multistage mass degradation, caused by the added starch. Tests in oxygen atmospheres instead of nitrogen showed no difference in the TGA curves. By considering the E_a plotted against the conversion rate or the TGA curves from the three aging conditions and the pure PLA, there is evidence that the starch or the starch in the composite degrades first compared to the pure PLA.[24] Considering Figures 4 and 5, the influence of the starch on the thermal behavior becomes clear. The earlier degradation of the starch (Figure 4) in TGA curves is reflected in a high E_a at low conversion rate. Above a conversion rate of 0.25%, which corresponds to a temperature of 300°C, the degradation of both components, the PLA and starch, can be seen. This leads to a decrease of the E_a in the PLA/starch composite as shown in Figure 5.

In all material characterization methods used, clear differences can be observed between the pure PLA and PLA/starch composite. The two materials examined differ considerably from each other, not only after accelerated aging but even in fresh molded condition. The measurement of the elongation at break by using a tensile test and a three-point bending test led to similar results. The temperature storage of the pure PLA samples caused a decrease in the elongation at break during the test period. The initial increase in elongation at break after 336 h can be explained by post-crystallization.[11] The DSC measurements confirm this. With a higher crystallinity degree of PLA, less continuous degradation occurs.[44,45] The glass transition temperature increases to 79.88°C during the 336 h temperature storage. Since physical aging is promoted near or above the glass transition temperature, no evident thermal degradation takes place either, since the storage temperature was 70°C. After 336 h, however, the glass transition temperature drops to 57.67°C. This promotes physical aging. The resulting accelerated relaxation and physical change of the material structure leads to cracks and deteriorated elongation.[11]

Humidity storage, on the other hand, increased the elongation at break. The underlying reason for this is the plasticizing effect of humidity on the PLA. This correlation has often been observed in connection with PLA and leads to plasticization or to an increased elongation at break by increasing the ductility.[46–48] Hydrolysis takes place

at an accelerated rate at high temperatures.[11,49] The high humidity but low storage temperature in combination do not show any degradation, that is, decreased elongation. This effect is also observed in the increased value of elongation at break in the standard climate, where the humidity was 50%. Regarding the elongation at break of the starch-filled specimens, no significant difference could be detected throughout all storage conditions. The compatibility between the hydrophilic starch and the hydrophobic PLA does not seem to change during the three different storages.

An increase in the impact strength of the pure PLA samples, caused by temperature storage, was detected. The samples were hardly measurable after temperature storage and slipped out of the sample clamps during testing, which explains the high standard deviation. Due to the increased crystallinity, the material seems to absorb more impact energy. The moisture in the air causes the impact strength to increase. For the starch-filled specimens, the cause of the increased impact strength after 792 h in temperature storage is the increased degree of crystallization. The decrease in impact strength in the humidity storage can be attributed to the swelling of the starch grains. As the starch grains absorb moisture, this leads to micro cracking, which then weakens the material to the point where the material cannot absorb much impact energy.[31] Similar behavior was seen for bio-Polyamide/regenerated cellulose fiber composites due to swelling and shrinkage of the fibers.[50]

Since the investigations have shown how beneficial starch as a filler is for the resistance of PLA, further investigations with regard to additives or coupling agents can improve the mechanical properties of the PLA/starch composite even with a high weight percentage of starch.

5 | CONCLUSIONS

The main purpose of this research was to investigate the aging behavior of PLA and PLA/starch composite in accelerated temperature and humidity aging conditions. Furthermore, the correlation between the E_a and the related mechanical, thermographic, and optical properties was investigated. It has been proven that both accelerated aging storages are stressful for the materials, which is reflected in a decrease of E_a during the experiments. This means that both materials are susceptible to degradation. The PLA/starch composite, however, slows down this rapid decrease of E_a. The results of the E_a demonstrate that the E_a of the composite does not change much over time depending on storage conditions, unlike pure PLA, which shows sharp drop in E_a in all storage conditions. The DSC measurements also show that starch as a filler leads to higher crystallization values when stored in high humidity, which is associated with higher resistance. In terms of elongation at break and impact strength, the pure PLA predominantly shows the better results. In comparison, however, the composite shows material property changes which are less pronounced and show very similar results across all storages. This once again demonstrates the advantages of composite materials.

Since a high E_a means that chemical reactions occur more gradually and indicate thermal stability, it was shown that native potato starch slows down the aging process and thus makes the material more resistant. As no additional additives or coupling agents were used in this research to investigate the effects of pure PLA and native potato starch, it is expected that additives or compatibilizers are used for this material composite, an improvement in the mechanical properties will occur.

ACKNOWLEDGMENTS

This research was funded by the Federal Ministry of Food and Agriculture (BMEL) and the Fachagentur Nachwachsende Rohstoffe e.V. (FNR): 2220NR089E. The authors would like to thank the companies TotalEnergies Corbion Emsland Stärke for providing the materials for this research. Open Access funding enabled and organized by Projekt DEAL.

CONFLICT OF INTEREST STATEMENT

The authors declare no conflict of interest.

DATA AVAILABILITY STATEMENT

The data that support the findings of this study are available from the corresponding author upon reasonable request.

ETHICS STATEMENT

No ethical approval was required for the investigations carried out, as no experiments were carried out with human tissue.

ORCID

Margarita Reit https://orcid.org/0000-0001-9879-3376

REFERENCES

[1] A. K. Trivedi, M. K. Gupta, H. Singh, *Adv. Ind. Eng. Polym. Res.* **2023**, *6*, 382.
[2] IfBB—Institute for Bioplastics and Biocomposites, Biopolymers—Facts and statistics 2022, 2023. https://www.ifbb-hannover.de/files/IfBB/downloads/faltblaetter_broschueren/f+s/Biopolymers-Facts-Statistics-einseitig-2022.pdf
[3] N. Karimpour-Motlagh, H. A. Khonakdar, S. M. A. Jafari, A. Mahjub, M. Panahi-Sarmad, S. F. Kasbi, S. Shojaei, V. Goodarzi, M. Arjmand, *Thermochim. Acta* **2020**, *691*, 178709.
[4] T. Chen, X. Zhao, Y. Weng, *Front. Chem.* **2022**, *10*, 1107620.
[5] N. Krug, J.-C. Zarges, H.-P. Heim, *Polymer* **2023**, *15*, 3461.
[6] V. DeStefano, S. Khan, A. Tabada, *Eng. Regener.* **2020**, *1*, 76.
[7] R. A. Ilyas, S. M. Sapuan, M. M. Harussani, M. Y. A. Y. Hakimi, M. Z. M. Haziq, M. S. N. Atikah, M. R. M. Asyraf, M. R. Ishak, M. R. Razman, N. M. Nurazzi, M. N. F. Norrrahim, H. Abral, M. Asrofi, *Polymer* **2021**, *13*, 1326.
[8] U. Meekum, A. Khiansanoi, *Results Phys.* **2018**, *8*, 79.
[9] R. Auras, B. Harte, S. Selke, *Macromol. Biosci.* **2004**, *4*, 835.
[10] R. A. Auras, B. Harte, S. Selke, R. Hernandez, *J. Plast. Film Sheet.* **2003**, *19*, 123.
[11] G. W. Ehrenstein, S. Pongratz, *Beständigkeit von Kunststoffen*, Hanser, München **2007**.
[12] S. Vyazovkin, *Molecules*, Vol. 25, MDPI, Basel, Switzerland **2020**, p. 25.
[13] "DIN 50035:2012–09"; Terms and definitions used on ageing of materilas- Polymeric materials. 2012.
[14] P. Budrugeac, *Polym. Degrad. Stab.* **1995**, *50*, 241.

[15] E. V. Bystritskaya, T. V. Monakhova, V. B. Ivanov, *Polym. Test.* **2013**, *32*, 197.
[16] I. S. Čubrić, G. Čubrić, I. Katić Križmančić, M. Kovačević, *Polymer* **2022**, *14*, *1682*.
[17] L. Cui, B. Imre, D. Tátraaljai, B. Pukánszky, *Polymer* **2020**, *186*, 122014.
[18] P. Müller, B. Imre, J. Bere, J. Móczó, B. Pukánszky, *J. Therm. Anal. Calorim.* **2015**, *122*, 1423.
[19] K. T. Gillen, R. Bernstein, M. Celina, *Rubber Chem. Technol.* **2015**, *88*, 1.
[20] D. Fadel, A. Laifa, R. Djamai, **2006**, https://www.semanticscholar.org/paper/Kinetics-of-degradation-of-photodegradable-films-by-Fadel-Laifa/006ce5853fe89093dc7c95b0e428103c603171cf.
[21] S. Reed, **2011**, https://www.semanticscholar.org/paper/A-study-of-the-manufacturing-and-product-of-a-cork-Reed/667fd3d8a3471d68ceb84fdeafd6ee5721d2bd00.
[22] T. Todhanakasem, Sorawit Panjapiyakul, P. Koombhongse, *Packag. Technol. Sci.* **2021**, *35*, 105.
[23] C. Martin, A. M. Smith, *Plant Cell* **1995**, *7*, 971.
[24] R. Acioli-Moura, X. S. Sun, *Polym. Eng. Sci.* **2008**, *48*, 829.
[25] K. Moraczewski, M. Stepczyńska, R. Malinowski, T. Karasiewicz, B. Jagodziński, P. Rytlewski, *Polymer* **2019**, *11*, 575.
[26] S. Zhang, Y. Liang, X. Qian, D. Hui, K. Sheng, *Nanotechnol. Rev.* **2020**, *9*, 524.
[27] B. Abderrahim, E. Abderrahman, A. Mohamed, T. Fatima, T. Abdesselam, O. Krim, *World J. Environ. Eng.* **2015**, *3*, 95.
[28] S. M. Aharoni, *J. Appl. Polym. Sci.* **1972**, *16*, 3275.
[29] O. Reinsdorf, C. Pellegrin, C. Schmidt, M. Alvear, K. Eränen, D. Y. Murzin, T. Salmi, *ChemCatChem* **2023**, *15*, 15.
[30] M. Stolov, V. Freger, *J. Membr. Sci.* **2023**, *678*, 121616.
[31] V. Goetjes, J.-C. Zarges, H.-P. Heim, *J. Appl. Polym. Sci.* **2023**, *141*, e54768.
[32] J. Fuchs Dr., *Fuchs-PLA-Stärke-Blends*. **2018**.
[33] J. H. Flynn, L. A. Wall, *J. Res. Natl. Bureau Standards Sect. A, Phys. Chem.* **1966**, *70A*, 487.
[34] T. Ozawa, *BCSJ* **1881**, *1965*, 38.
[35] Z. Alhulaybi, I. Dubdub, M. Al-Yaari, A. Almithn, A. F. Al-Naim, H. Aljanubi, *Polymer* **2022**, *15*, 12.
[36] J. Li, W. Zheng, L. Li, Y. Zheng, X. Lou, *Thermochim. Acta* **2009**, *493*, 90.
[37] J. O. Akindoyo, M. D. Beg, S. Ghazali, H. P. Heim, M. Feldmann, *Compos. A: Appl.Sci. Manuf.* **2017**, *103*, 96.
[38] S. Lv, J. Gu, H. Tan, Y. Zhang, *J. Cleaner Prod.* **2018**, *203*, 328.
[39] M. A. Sawpan, K. L. Pickering, A. Fernyhough, *Compos. A: Appl.Sci. Manuf.* **2011**, *42*, 310.
[40] F. Carrasco, O. Santana Pérez, M. L. Maspoch, *Polymer* **2021**, *13*, 3996.
[41] Z. Yang, H. Li, Y. Duan, R. Zhang, Y. Zhang, X. Wang, *J. Mater. Sci.: Mater. Electron.* **2021**, *32*, 16194.
[42] Å. Nyflött, Ç. Meriçer, M. Minelli, E. Moons, L. Järnström, M. Lestelius, M. G. Baschetti, *J. Coat. Technol. Res.* **2017**, *14*, 1345.
[43] A. Kulkarni, R. Narayan, *Polymer* **2021**, *13*, 4125.
[44] M. Yu, Y. Zheng, J. Tian, *RSC Adv.* **2020**, *10*, 26298.
[45] B. Ma, X. Wang, Y. He, Z. Dong, X. Zhang, X. Chen, T. Liu, *Polymer* **2021**, *212*, 123280.
[46] A. M. Harris, E. C. Lee, *J. Appl. Polym. Sci.* **2010**, *115*, 1380.
[47] T. Mekonnen, P. Mussone, H. Khalil, D. Bressler, *J. Mater. Chem. A* **2013**, *1*, 13379.
[48] N. Jia, V. A. Kagan, in *Plastics Failure: Analysis and Prevention* (Ed: J. Moalli), Plastics Design Library, Norwich, NY **2001**, p. 95.
[49] S. Muroga, Y. Hikima, M. Ohshima, *Appl. Spectrosc.* **2017**, *71*, 1300.
[50] C. K. Falkenreck, N. Gemmeke, J.-C. Zarges, H.-P. Heim, *Polymer* **2023**, *15*, 1606.

How to cite this article: M. Reit, J.-C. Zarges, H.-P. Heim, *Biopolymers* **2024**, *115*(3), e23571. https://doi.org/10.1002/bip.23571